Acta Materialia 274 (2024) 119996

Contents lists available at ScienceDirect

Acta Materialia

journal homepage: www.elsevier.com/locate/actamat

Excellent intrinsic magnetic properties in the $TbCu_7$-type Sm-Fe-N compound

A.R. Dilipan [a,b], D. Ogawa [a], H. Sepehri-Amin [a,b], P. Tozman [a], T. Hiroto [a], K. Hono [a,b], Y. K. Takahashi [a,*]

[a] National Institute for Materials Science, Tsukuba 305-0047, Japan
[b] Graduate School of Science and Technology, University of Tsukuba, Tsukuba 305-8577, Japan

ARTICLE INFO

Keywords:
Intrinsic magnetic properties
$TbCu_7$-type $SmFe_9$
Permanent magnetic thin films

ABSTRACT

We report excellent intrinsic magnetic properties of $SmFe_9N_\delta$ epitaxial thin films with $TbCu_7$-type crystal structure, i.e., room temperature saturation magnetization ($\mu_0 M_s$) of 1.64 T, Curie temperature (T_c) of 771 K and magnetic anisotropy field ($\mu_0 H_A$) of ~22 T for δ=1.1, the saturation magnetization of which is superior to that of $Sm_2Fe_{17}N_3$ ($\mu_0 M_s$= 1.57 T) and $Nd_2Fe_{14}B$ compounds ($\mu_0 M_s$= 1.61 T). X-ray diffraction and transmission electron microscopy revealed that the thin films have a highly textured single $TbCu_7$-type phase with its *c*-axis perpendicular to the film. Heat treatment of the thin films under N atmosphere expands the lattice and increases the unit cell volume of the $SmFe_9N_\delta$ structure, which also switches the magnetocrystalline anisotropy from easy plane (δ = 0) to easy axis (δ=1.1). Furthermore, the $\mu_0 M_s$ and T_c of $SmFe_9N_\delta$ films also increased with increasing nitrogen content in the structure, leading to promising intrinsic magnetic properties. Based on this study, we can conclude that the rare-earth lean $SmFe_9N_\delta$ based $TbCu_7$-type compound has potential for the development of high performance anisotropic bonded magnets with superior performance to that of existing anisotropic $Sm_2Fe_{17}N_3$ or Nd-Fe-B bonded magnets.

1. Introduction

In sustainable/clean energy-driven technologies such as hybrid/electric vehicles and wind turbines, permanent magnets play a key role as components in motors and generators. (Nd, Dy)-Fe-B magnets are predominantly used for these applications due to their high maximum energy product [1,2]. However, the increasing demand and the high supply risk of Nd and Dy have recently created the urge to find an alternative permanent magnet [3]. Sm-Fe based compounds have been considered as potential for an alternative permanent magnet (PM), as some of these compounds require a lower content of rare earth (RE) elements, and one can reduce the complete dependence on Nd and Dy sources [4].

Various Sm-Fe-based compounds are summarized in Table 1. The $SmFe_5$ compound has the $CaCu_5$-type structure, where the Sm atoms of this structure can be substituted with different amounts of dumbbell pairs of Fe leading to the formation of Sm_2Fe_{17}, $SmFe_9$ and $SmFe_{12}$ compounds. Among these, the $ThMn_{12}$-type $SmFe_{12}$ (1:12) compound with a tetragonal crystal structure has gained a lot of attention recently as it has the highest Fe content [5] in the rare earth-based compounds. However, the 1:12 compounds are unstable in bulk form and require a large amounts of stabilizing elements like Ti and V to be substituted for Fe, which deteriorates the intrinsic magnetic properties, especially the saturation magnetization ($\mu_0 M_s$) [6]. Another candidate with high Fe content is the metastable $TbCu_7$-type Sm-Fe (1:7) compound of hexagonal crystal structure with the space group of P6/*mmm*. In the 1:7 structure, Sm atoms are randomly substituted by a dumbbell of Fe atoms in a disordered manner. This disordered structure of the 1:7 compound makes it interesting because the Fe atoms in the 1:7 structure can be accommodated beyond the stoichiometry of $SmFe_7$, i.e., Fe:Sm > 7 [7,8]. Thus, $\mu_0 M_s$ in the 1:7 compound can be altered [9,10].

Although the 1:7 compound can have a high magnetization by increased Fe content, the 1:7 system has received very little attention due to the existing thermodynamically stable Th_2Zn_{17}-type Sm_2Fe_{17} (2:17) compound. In 2:17, the Sm atom is replaced by the dumbbell of the Fe atom in an ordered manner. Nitride of the 2:17 compound, i.e., $Sm_2Fe_{17}N_3$ phase, exhibits uniaxial anisotropy with good intrinsic magnetic properties [12]. However, the $\mu_0 M_s$ of the 2:17 phase is limited

* Corresponding author.
E-mail address: takahashi.yukiko@nims.go.jp (Y.K. Takahashi).

https://doi.org/10.1016/j.actamat.2024.119996
Received 5 December 2023; Received in revised form 3 April 2024; Accepted 9 May 2024
Available online 10 May 2024

Table 1
Characteristics of Sm-Fe-based compounds with different crystal structures [7, 11,12].

Compound	Structure-type	Crystal structure	Phase stability	Anisotropy type
$SmFe_5$	$CaCu_5$	Hexagonal	Unstable	Uniaxial after nitridation
Sm_2Fe_{17}	Th_2Zn_{17}	Trigonal	Stable	Uniaxial after nitridation
$SmFe_9$	$TbCu_7$	Hexagonal	Metastable	Uniaxial after nitridation
$SmFe_{12}$	$ThMn_{12}$-type	Tetragonal	Unstable	Uniaxial

to 1.57 T, which is lower than that of the Nd-Fe-B compound (1.61 T). Similar to the 2:17 compounds, 1:7 compounds in a nitride form acquire uniaxial anisotropy [13–15]. The maximum $\mu_0 M_s$ of 1.7 T is achieved in the 1:7 compounds [16], which is higher than that of Nd-Fe-B and other existing stable Sm-Fe compounds. Moreover, unlike the 1:12 compound, the 1:7 compound is advantageous as it can be stabilized in bulk form by non-equilibrium processing, such as, melt-spinning, rapid quenching, HDDR, and mechanical alloying, without the addition of stabilizing elements [10,17–19]. Overall, the high Fe content and a resulting high magnetization along with the ability to be processed in bulk form without the need for stabilizers make the $SmFe_9$-based compound a potential candidate for the development of alternative permanent magnetic material, which can be processed into anisotropic bonded magnets and sintered magnets. However, this compound is not well explored, and its intrinsic magnetic properties are unknown.

In this study, we revisit the $TbCu_7$-type $SmFe_9$-based compounds and evaluate their intrinsic magnetic properties, such as, $\mu_0 M_s$, Curie temperature (T_c), and anisotropy field ($\mu_0 H_A$). To measure the exact values of the intrinsic magnetic properties for any ferromagnetic compound, single phase and highly textured sample is required and the best way to obtain this is to grow epitaxial thin films. Recently, Kusumori *et al.* fabricated epitaxial/textured 1:7 thin films and its nitrides, but were unsuccessful in obtaining uniaxial anisotropy upon nitriding the 1:7 phase [20]; they reported magnetocrystalline anisotropy type to be in the 'easy-plane' and 'easy-cone' state. Katter *et al.* [15] estimated the anisotropy field of $TbCu_7$-type $Sm_{10.6}Fe_{89.4}N_x$ to be ~8.6 T in an isotropic powder, but the nitrogen content was not quantified. The nitrogen content plays an essential role in the intrinsic magnetic properties of 1:7 and 2:17 compounds. Iriyama *et al.* studied the effect of nitrogen content on $Sm_2Fe_{17}N_x$ ($0 < x < 6$) and found that $x = 3$ shows the highest $\mu_0 H_A$ of 22 T [21,22]. So far, there is no systematic study on this relationship in highly textured 1:7 compounds.

Compared to other rapid solidification and single crystal growth methods, thin film synthesis enables the growth of metastable phases with fewer defects and in a single phase. Additionally, thin films can be nitrided more homogeneously, and their nitrogen content can be determined more accurately compared with powder forms. Because powders often show non-uniform nitrogen distribution with a certain penetration depth depending on nitrogen pressure and temperature [23, 24]. On the other hand, thin films offer a uniform matrix that allows analysis across the entire sample and facilitates precise measurement of nitrogen distribution. In this article, we report the comprehensive intrinsic magnetic properties of the $TbCu_7$-type Sm-Fe compound and its nitrides in epitaxial thin film form. A $\mu_0 H_A$ of ~ 22 T, which is higher than Nd-Fe-B and comparable to that of $Sm_2Fe_{17}N_3$ compounds, along with a high $\mu_0 M_s$ of 1.64 T and a T_c of 771 K were achieved. The excellent intrinsic magnetic properties determined in this study make the $TbCu_7$-type $SmFe_9$-based compound a potential candidate for an anisotropic bonded magnet with potential superior performance compared to the existing ones.

2. Experimental

$TbCu_7$ type $SmFe_9N_\delta$ with various nitrogen concentrations, $\delta = 0$, 0.5, 0.7, and 1.1, were fabricated using an ultra-high vacuum magnetron sputtering system (Comet, Inc., CMS-3200) with the base pressure of 10^{-7} Pa. To obtain *c*-axis texture, the thin films were grown on a single-crystalline Al_2O_3 (0001) substrate with a Mo buffer layer at 350 °C, as schematically shown in Fig. 1. The Al_2O_3 substrate was annealed at 1000 °C for 1 hour to minimize the surface miscut effect, which eventually improves substrate surface smoothness and the thin film texture [25]. A 30 nm thick Mo buffer layer was deposited on the Al_2O_3 substrate. Mo (111) layer was epitaxially grown on the Al_2O_3 substrate. In contrast to previous work using Ta as the buffer layer [20], Mo was used here because it can develop the (111) orientation at room temperature, unlike the elevated temperatures for Ta. Nitridation was performed at 350 °C after the deposition of the Sm-Fe layer, by flowing high-purity nitrogen gas at the flow rate of 50 sccm, while varying the chamber pressure from 2 to 10 Pa. The thin film with different nitrogen content from 0 to 10 at.% was obtained. After the formation of the $SmFe_9N_\delta$ layer, the Mo capping layer was deposited to avoid surface damage and oxidation. Fig. 1 shows the typical film structure thus grown, Al_2O_3 (0001) || Mo (111) || Sm-Fe (1:7) (0001) || Mo-capping.

The microstructure of the films, their composition, and nitrogen concentration were studied using an aberration corrected scanning transmission electron microscopy (STEM) (FEI TitanG2 80–200) coupled with the energy dispersive X-ray spectroscopy (EDS) using FEI-Super-X EDX detector. According to the nitrogen atomic concentration which is determined from EDS, the thin films are labeled as SFN0 (0 at.% for $\delta = 0$), SFN5 (5.6 at.% for $\delta = 0.5$), SFN7 (7.2 at.% for $\delta = 0.7$) and SFN10 (10.0 at.% for $\delta = 1.1$) and its respective composition is mentioned in supplementary Table S1. The electron transparent specimens for TEM analysis were prepared by the focused ion beam (FIB) lift-out technique using FEI Helios G4-UX. The crystal structure, phase, and texture characterization were performed using X-ray diffraction (XRD) (Rigaku, SmartLab) with a 2D detector (Rigaku, PILATUS100K/R and HyPix-3000).

The room temperature magnetic properties were measured by physical property measurement system (PPMS) with the VSM option (Quantum Design Inc. Dynacool) under a maximum applied magnetic field of 14 T. The temperature-dependent magnetic properties of the thin films were measured using a 7 T magnetic field superconducting quantum interference device (SQUID) magnetometer (Quantum Design Inc. MPMS) at temperature range of 50–750 K. The Curie temperature of the thin films was estimated using the nonlinear least-squares fitting proposed by Kuz'min et al.,[26]

The first and second order magnetocrystalline anisotropy constants, K_1 and K_2 were estimated using the anomalous Hall effect (AHE) torque method demonstrated by Ono *et al.*, [27] using PPMS at the magnetic field of 14 T at different sample orientations.

3. Results and discussion

3.1. Crystallography and phase identification

Fig. 2a represents the out-of-plane XRD pattern obtained for thin films with various nitrogen contents SFN0, SFN5, SFN7 and SFN10, where the 0, 5, 7, 10 represent atomic percentage of nitrogen in the thin films. The Al_2O_3 and Mo peaks that correspond to the substrate and the buffer layer respectively; the Mo layer is oriented with the (111) plane along the substrate surface. In the SFN5, SFN7, and SFN10 nitride films, the 000*l* peaks of the 1:7 phase shift gradually towards the low 2θ angle, which indicates the expansion of the lattice upon nitrogen diffusion into the interstitial sites. The 0002 peaks of all the thin films are shown in detail in Fig. 2b, where the shift upon the nitrogen treatment is clearly seen. The largest peak shift was observed for the SFN10 sample with respect to the SFN0 sample, caused by its high nitrogen content. No peak

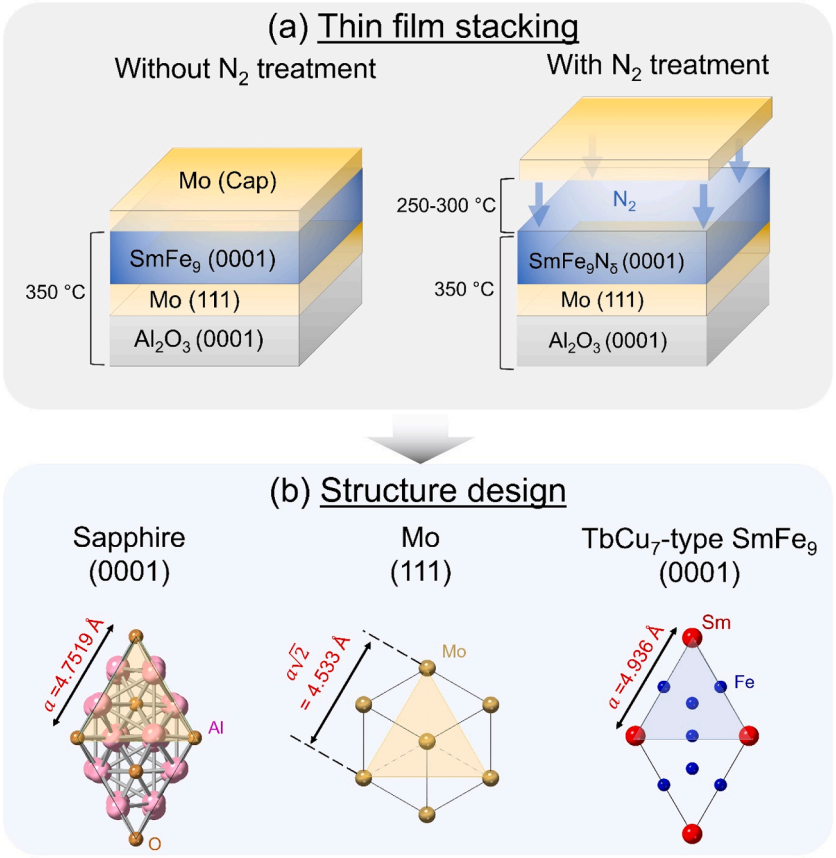

Fig. 1. (a) A schematic illustration of $TbCu_7$-type $SmFe_9$ and its nitridation process for $SmFe_9N_\delta$ (b) Thin film structure design for the compatibility of Al_2O_3 substrate, Mo buffer layer and $SmFe_9$ with its lattice constant matching.

shift is observed for the Mo 222 peak and the Al_2O_3 0001 peak upon nitriding, indicating that the N-atoms enter only the 1:7 phase. The nitrogen doping increases the lattice parameters *a* and *c* as represented in Fig. 2c. A systematic increase in the unit cell volume from 0.086 nm^3 for SFN0 to 0.090 nm^3 for SFN10 can be seen. Moreover, the axial ratio, *c/a,* increases with increasing nitrogen content, from 0.855 for SFN0 to 0.870 for SFN10, which also indicates the significant expansion towards *c*-axis (Fig. 2c).

To further verify the existence of the hexagonal 1:7 phase, Azimuthal scans (ϕ-scan) were performed and presented for the SFN10 film in Fig. 3a and 3b. The ϕ-scan was measured at 2θ=48.63° and χ=62.73° which corresponds to {201} lattice planes of 1:7 phase. A 6-fold symmetry is attributed to the hexagonal structure, confirming the presence of the 1:7 phase and denotes that the thin film possesses a good epitaxy. Due to the structural similarities of the 2:17 and 1:7 phases, it is important to confirm the absence of the 2:17 phase by checking its superlattice peak reflection. The ϕ-scan was measured at 2θ=25.05° and χ=73.41°, which corresponds to the {021} superlattice reflection of the 2:17 phase and presented in Fig. 3b. No peaks attributed to the 2:17 phase was observed confirming its absence and satisfying the formation of 1:7 as the main layer phase [20]. A schematic representation of different rotation angles of sample stage in XRD such as χ, ϕ, ω, 2θ is mentioned in Fig. 3c.

3.2. Room temperature magnetic properties

Fig. 4 shows the room temperature magnetization hysteresis curves of SFN0 (a), SFN5 (b), SFN7 (c) and SFN10 (d) measured with the field direction along the film (//) and perpendicular to the film (⊥). As can be seen from the XRD profile, the film has good epitaxial growth with the *c*-axis perpendicular to the film. Without nitriding (SFN0), the *M-H* loop shows that easy magnetic axis (EMA) is in the plane, showing the planar anisotropy along the *ab*-plane. Whereas, the *M-H* loops of the SFN10 sample show the EMA along ⊥ measurement, representing uniaxial anisotropy along the *c*-axis. The anisotropy type switches from easy-plane to easy-axis anisotropy as nitrogen content increases. It can be seen that the optimization of N content is important to achieve the uniaxial anisotropy. In general, the interstitial doping with B, N, and C creates a strong uniaxial anisotropy in several rare earth iron compounds [28,29]. These interstitial atoms are positioned close to the rare earth atoms, such that they create a strong crystalline electric field at the 4*f* electron sites. This systematic strengthening of the crystalline electric field gradient at rare-earth site can be the reason for the increasing magnetocrystalline anisotropy as the nitrogen content increases [30]. Moreover, it is seen that μ_0M_s increases with increasing nitrogen content in the structure. The μ_0M_s of SFN5 and SFN7 are 1.38 T and 1.46 T, respectively, which is higher than that of the SFN0 sample (1.22 T). The SFN10 sample with the uniaxial anisotropy has a high μ_0M_s of 1.64 T. The improvement in the μ_0M_s of nitride films corresponds to the lattice expansion and resulting changes in the electronic structure of sublattices upon interstitial nitrogen doping [28]. The μ_0M_s value of the SFN10 sample is higher than those of $Sm_2Fe_{17}N_3$ and $SmFe_{12}$ [5,31]. Overall, it can be seen from the *M-H* loops that the μ_0M_s increases, and the magnetocrystalline anisotropy type changes from planar to uniaxial with increasing nitrogen content in the 1:7 phase. Further analysis is needed to quantify the magnetocrystalline anisotropy field (μ_0H_A) value for the uniaxial SFN10 sample.

By finding the cross-point of the extrapolated // and ⊥ loops of the SFN10 sample, the μ_0H_A is estimated to be ~24 T, as shown in Supplementary Fig. S1. However, cross-point estimation is known to overestimate the μ_0H_A [32]. So, the anomalous Hall effect (AHE) torque experiment was adopted for accurate estimation of anisotropy constants

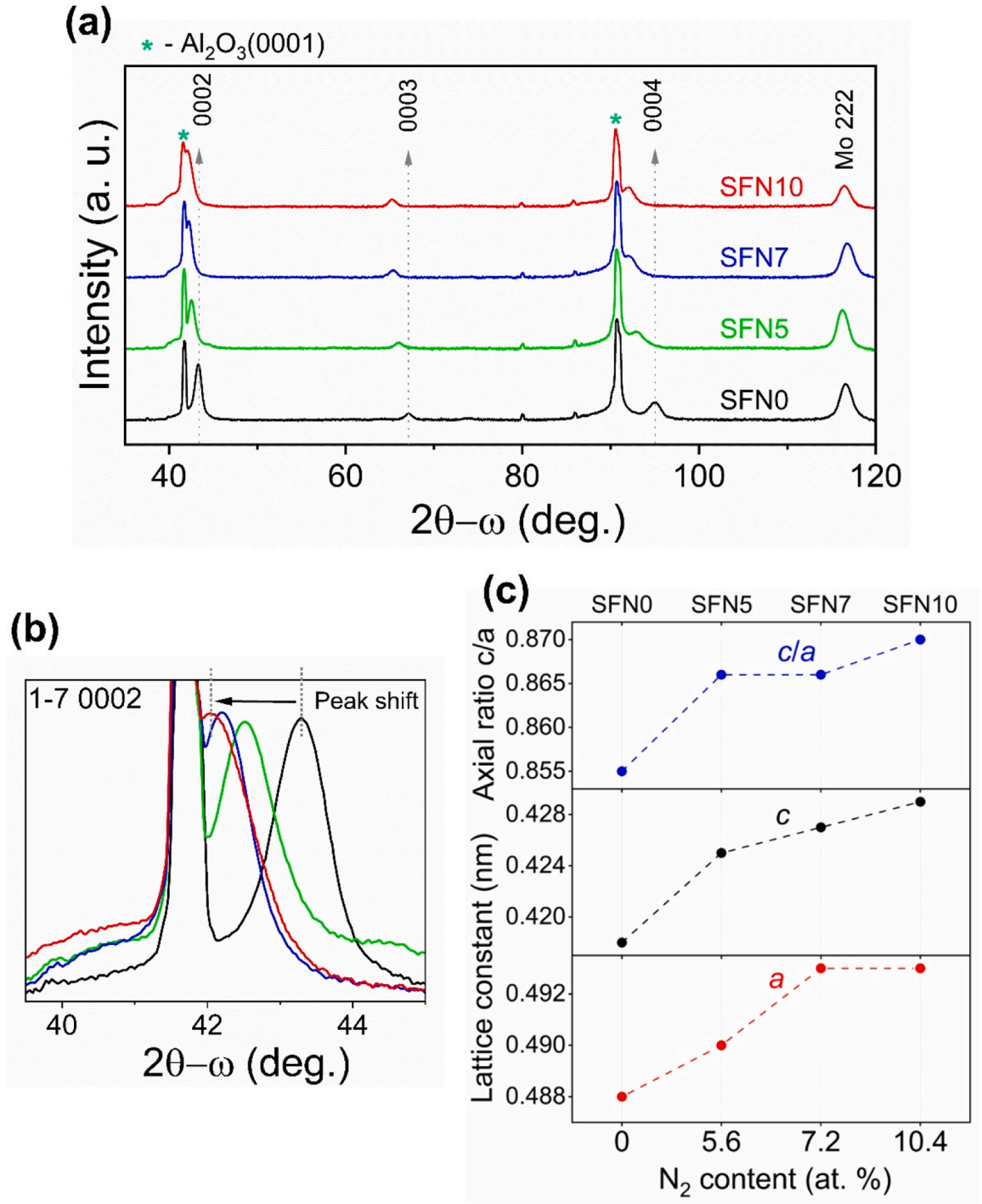

Fig. 2. (a) Out-of-plane X-ray diffraction patterns of SFN0, SFN5, SFN7 and SFN10 thin films. (b) Enlarged 0002 peaks of 1:7 phase representing peak shift by nitridation. (c) Lattice constant of all the thin films and its axial ratio.

(K_1 and K_2) and $\mu_0 H_A$. The K_1 and K_2 of nitride thin film were extracted from the AHE torque curve (Fig. S2) using the method demonstrated by Ono *et al.* [27] and mentioned in the Table 2. It can be seen that the SFN10 ($SmFe_9N_{1.1}$) show K_1 = 19.1 MJ/m^3 and K_2 = −2.2 MJ/m^3, which deduced a $\mu_0 H_A = (2K_1+4K_2)/M_s \sim 22.6$ T. A similar anisotropy of 22 T is determined also for $Sm_2Fe_{17}N_3$ powders with the anisotropy constant of K_1 =6.6 MJ/m^3 and K_2 = 3.3 MJ/m^3 [22]. The variation in these anisotropy constants could be attributed to the different crystal structures, 2:17 and 1:7 phases, of the similar compositions. The SFN7 and SFN5 show a less $\mu_0 H_A$ of ~12.9 and ~9.6 T respectively. Katter *et al.* [15] estimated the anisotropy field for $TbCu_7$-type $SmFe_{\sim 8}N_x$ to be 8.6 T, which is similar to those of the samples with low nitrogen content (SFN5 and SFN7). The $\mu_0 H_A$ obtained in SFN10 is greater than $Nd_2Fe_{14}B$ and is on par with $Sm_2Fe_{17}N_3$ [21]. Additionally, a coercivity of ~0.8 T is observed in the nitride thin films. This could be attributed to various factors like the increased anisotropy field, Sm-rich inhomogeneities in the microstructure and the low angle grain boundaries, which are usually observed in the Sm-Fe based epitaxial thin films [33,34].

3.3. Temperature dependent magnetic properties

In order to determine the Curie temperature (T_c), the *M-H* loops were

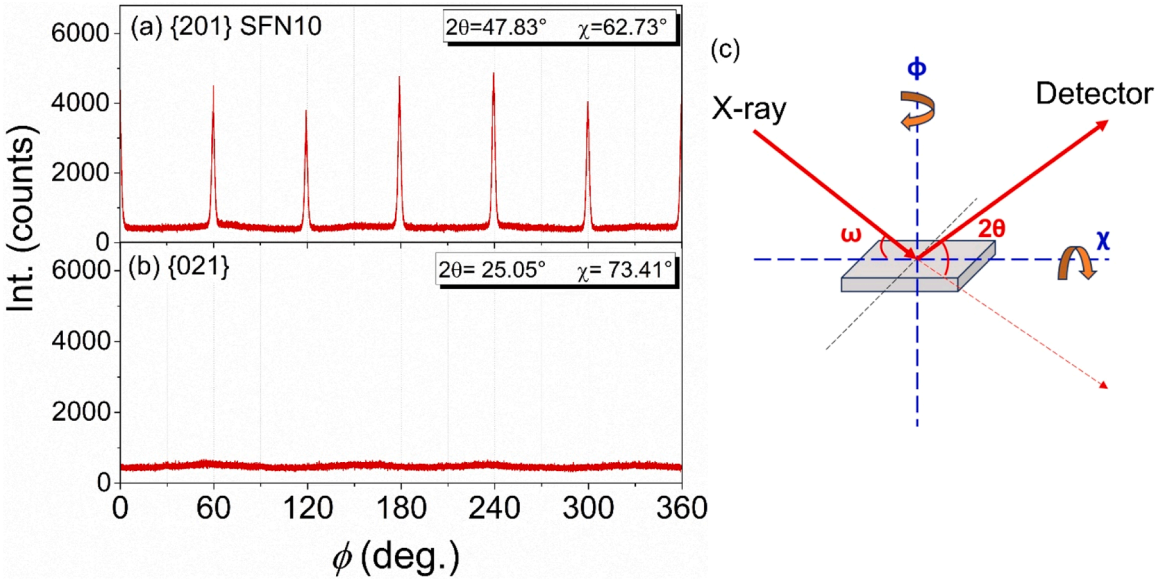

Fig. 3. (a) Azimuthal scan (ϕ scan) of SFN10 measured at 2θ=47.83° and χ=62.73° for {201} peak of 1:7 phase and (b) at 2θ= 25.05° and χ=73.41° for superlattice {021} peak of 2:17 phase. (c) schematics of thin film rotation angle with respect to incident X-ray.

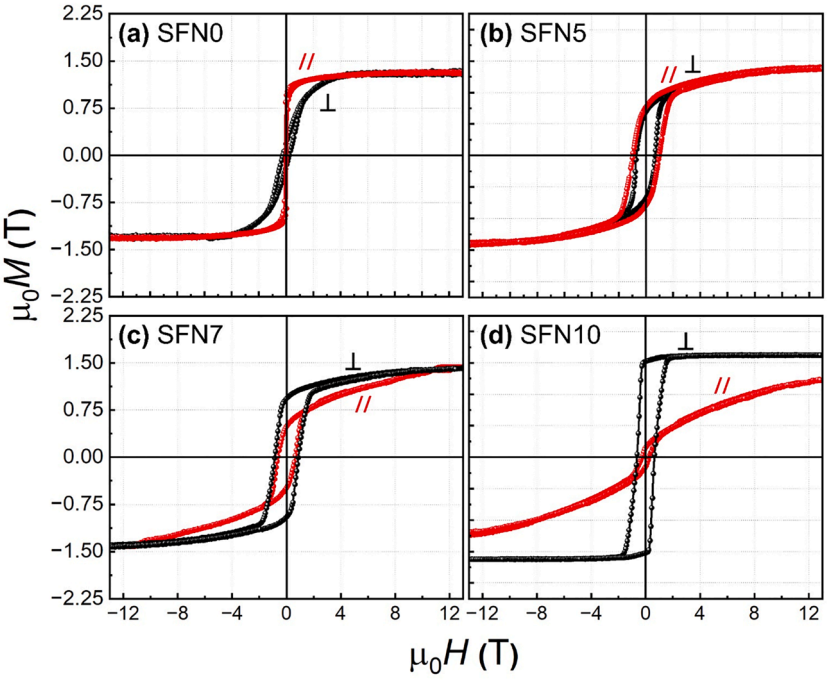

Fig. 4. M vs H hysteresis curves of (a) SFN0, (b) SFN5, (c) SFN7 and (d) SFN10 thin film measured parallel (//) and perpendicular (⊥) to the field direction with respect to the thin film surface.

Table 2
Intrinsic magnetic properties of nitride thin films measured at 300 K and estimated from $\mu_0 M_s$ vs. T.

Compound	$\mu_0 M_s$ (T)	$\mu_0 H_A$ (T)	K_1 (MJ/m^3)	K_2 (MJ/m^3)	T_c (K)
SFN5 ($SmFe_9N_{0.5}$)	1.38	9.6	10.6	−2.8	700
SFN7 ($SmFe_9N_{0.7}$)	1.46	12.9	12.3	−2.4	730
SFN10 ($SmFe_9N_{1.1}$)	1.64	22.6	19.1	−2.2	771

measured with respect to temperature (T) to obtain the $\mu_0 M_s$ vs. T in Fig. 5a. The T_c was estimated by extrapolating the $\mu_0 M_s$-T curve using least square fitting by the method demonstrated by Kuzmin *et.al.*[26]. The marker dots indicate the experimental curve and the dotted line indicates the extrapolated fitting.

T_c systematically increases from 501 K for SFN0 to 771 K for SFN10. For the SFN5 and SFN7 samples, the T_c is 700 K and 730 K, respectively. The high T_c in the nitride samples compared to the one without nitrogen can be caused by several factors like an increase in the $\mu_0 M_s$, enhanced Fe-Fe exchange interaction, and hybridization of N with Fe states owing to the interstitial N doping and volume expansion [38].

To get an overall understanding, the temperature dependence of

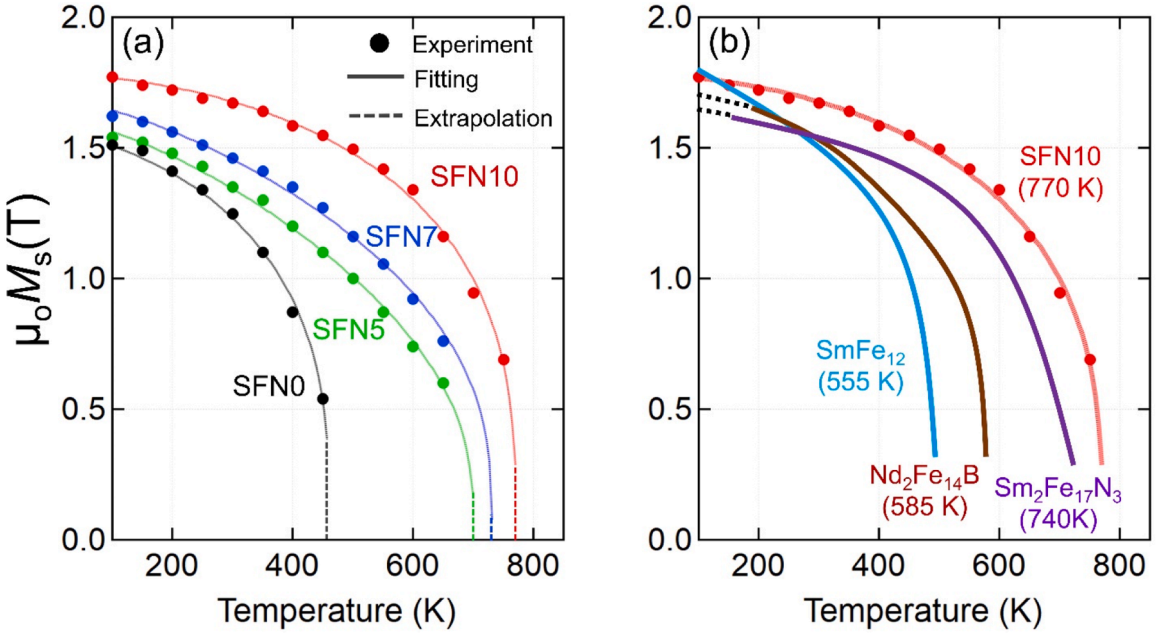

Fig. 5. (a) $\mu_o M_s$ vs T measured for all the thin films (b) $\mu_o M_s$ vs T of the SFN10 compared with $Sm_2Fe_{17}N_3$, $Nd_2Fe_{14}B$ and $SmFe_{12}$ [2,5,19,35–37].

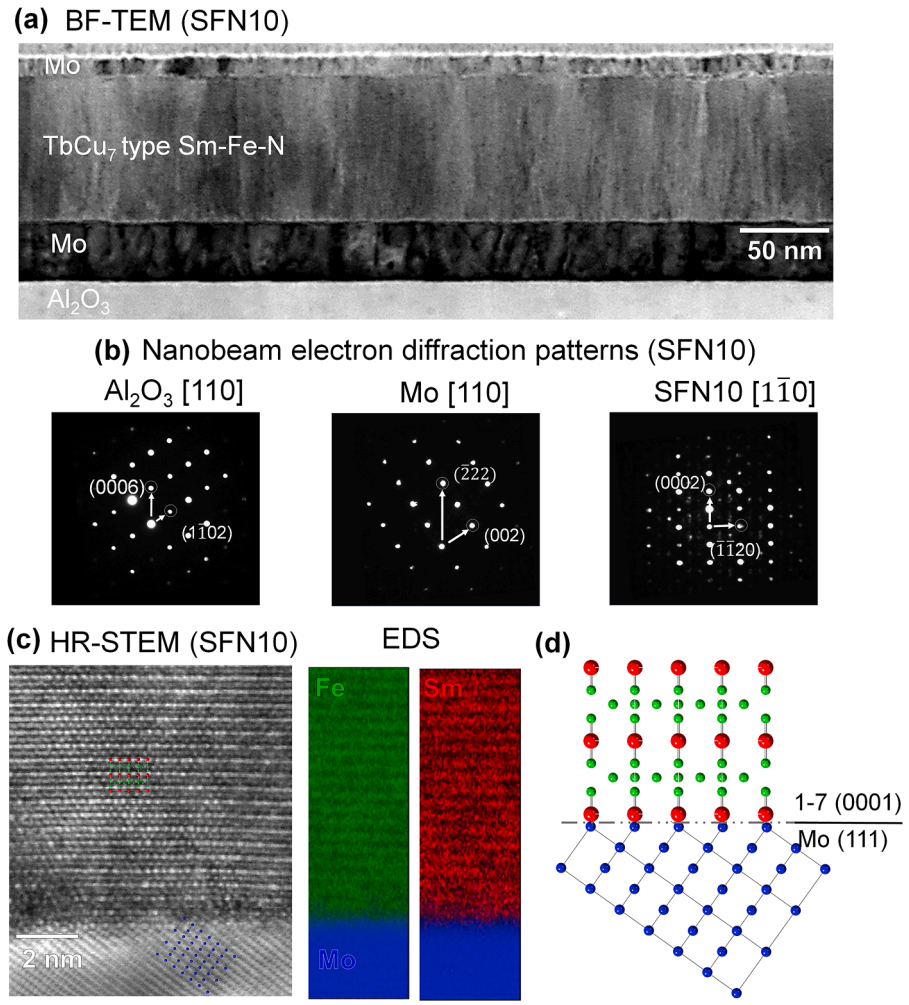

Fig. 6. (a) Cross-sectional BF-TEM images of SFN10 thin film with the stacking of Al_2O_3 (0001) || Mo (111) || 1:7 (0001) || Mo-capping. (b) Nano-beam diffraction pattern representing zone axis of Al_2O_3 [110], Mo [110] and 1:7 [1$\bar{1}$0]. (c) HR-STEM magnified images with its respective EDS maps. (d) Illustration of the atomic model of the interface.

$\mu_0 M_s$ for the SFN10 sample of this work is presented along with the various undoped RE-Fe based hard magnetic compounds shown in Fig. 5b. It is already known that the nitrides of 1:7 phase possess high thermal stability, when compared to $Sm_2Fe_{17}N_3$ [19,36,39], and the T_c of SFN10 (771 K) is higher than those of the $Sm_2Fe_{17}N_3$ (740 K) and other compounds ($SmFe_{12}$ and $Nd_2Fe_{14}B$) [2,5] showing the promise of the 1:7 based compound for elevated temperature applications. Further improvement of the T_c can be expected by the addition of Co, Zr, V, Nb and Ti into the 1:7 phase as reported elsewhere [13,14,39–42]. As the SFN10 sample has attractive $\mu_0 M_s$, $\mu_0 H_A$ and T_c, the microstructure of this sample is studied to understand the phase formation and to know the composition distribution of the thin film.

3.4. Interface and nano-chemistry

Fig. 6a shows the cross-sectional bright-field (BF) TEM image of the SFN10 thin film. It is seen that all the layers in the thin film stack (Al_2O_3 || Mo ||1:7 || Mo-capping), maintain sharp and flat interfaces. The average thickness of the main 1:7 layer is estimated to be 70±2 nm. Moreover, the 1:7 layer exhibits columnar growth, observed from the bright field (BF)-TEM image. The contrast of the 1:7 layer is originated from the low-angle grain boundaries. The existence of these nano-structural defects can be the reason for obtained coercivity, which is only 3.5% of the magnetic anisotropy field of matrix phase. The phase and its orientation were found from nano-beam electron diffraction patterns (Fig. 6b). The diffraction pattern from the substrate and buffer layer was found to be the [110] zone axis of Al_2O_3 and [110] zone axis of bcc-Mo, and the main layer belongs to the [$1\bar{1}0$] zone axis of the $TbCu_7$-type Sm-Fe phase. The orientation of Mo was found to be with the [111] axis perpendicular to the film surface, while the orientation of the 1:7 phase is with the [0001] perpendicular to the film surface. These nano-beam electron diffraction patterns are consistent with that of the XRD profile.

The high-resolution high angle annular dark field (HAADF) STEM images and its respective EDS observed near the interface of the Mo buffer layer and magnetic layer (Fig. 6c) reveal that the $(111)_{Mo}$ matches with the main layer's (0001) plane, which is on par with the atomic model of the interface (schematically represented in Fig. 6d). The lattice mismatch for the (111) plane of Mo and (0001) plane of the 1:7 phase is low ~8 %; this is the reason for the preferential growth direction of the 1:7 layer.

To study the composition distribution and possible presence of secondary phases in the SFN10 film, STEM-EDS map was collected over a large region of the film. Fig. 7 shows the panoramic HAADF image, and the STEM-EDS mapping with a corresponding line profile for the cross-sectional sample of SFN10 thin film. The STEM-EDS elemental maps in Fig. 7b and the line profile show overall uniform compositions throughout the film with negligible traces of Sm rich agglomerates near the buffer layer interface. These inhomogeneities could also be the reason for the obtained coercivity, which is usually observed in Sm-Fe based thin films [33,34,43,44]. The elemental EDS line profile (Fig. 7b) shows that the interface of the 1:7 layer with the Mo layer is relatively flat and no diffusion of Mo into the main phase or the formation of Mo-Fe or Mo-Sm based intermetallic phases are seen. The chemical composition of the SFN10 was estimated to be $SmFe_{8.8}N_{1.1}$. Although the composition contains higher Fe content beyond the

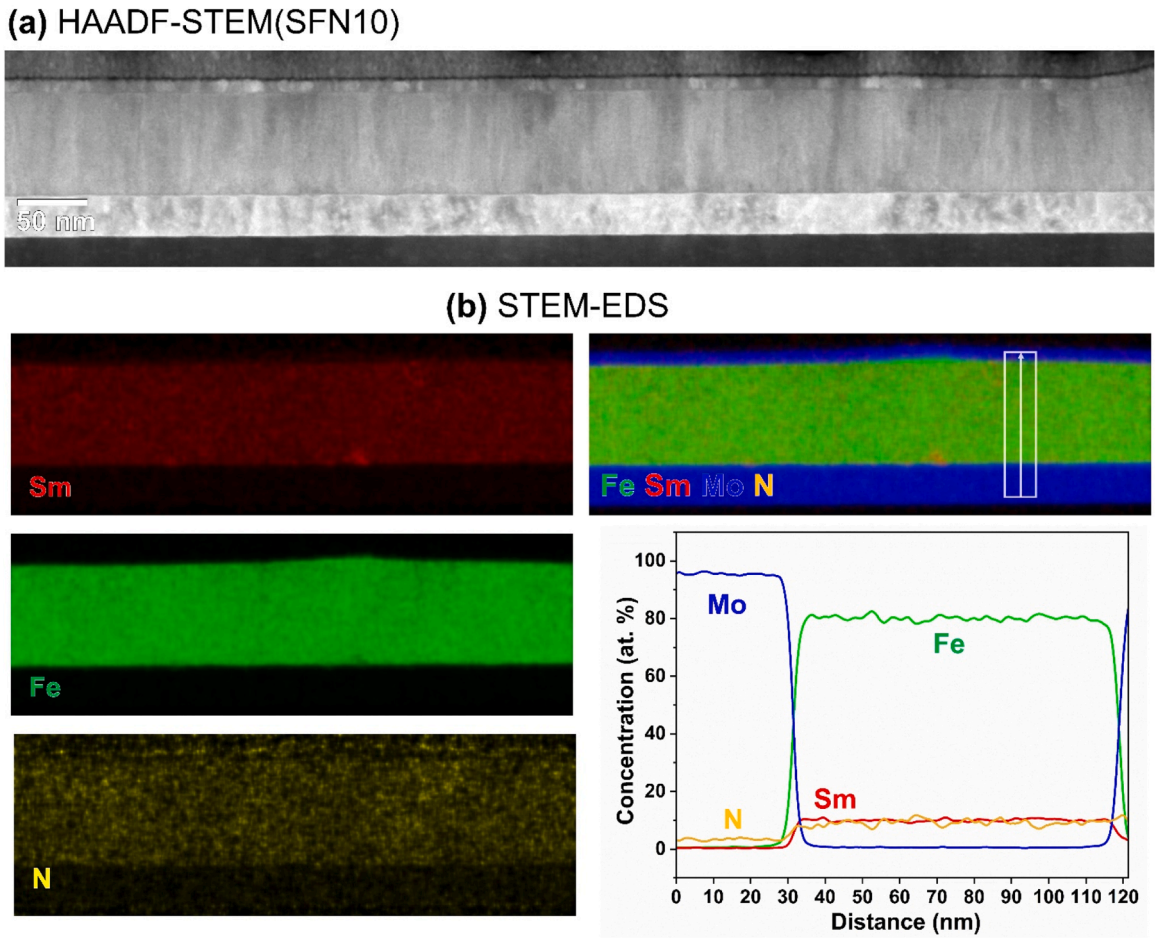

Fig. 7. (a) Cross sectional panoramic HAADF-STEM image of SFN10 and (b) respective EDS maps of each element of the main and buffer layer with its the line profile.

stoichiometry of 1:7, the predominantly occurring α-Fe phase reaction layer or segregates in the previously reported Sm-Fe based thin films, are not observed. The magnetic phase purity is important in determining the intrinsic magnetic properties, as the soft magnetic phases like α-Fe causes the overestimation the $\mu_o M_s$ value [45]. The nitrogen dissolution can be observed from the N elemental map in the main layer without affecting the Mo buffer and capping layer. From the overall TEM observation, the SFN10 thin film possess single 1:7 phase without any secondary ferromagnetic phases.

3.5. $\mu_0 M_s$ vs. $\mu_0 H_A$ and T_c of PM compounds

Fig. 8 summarizes the three important intrinsic magnetic properties ($\mu_0 M_s$, $\mu_0 H_A$ and T_c) of several hard magnetic phases reported in literatures [2,11,12,21,22,37,43,46–59] and the position of the $Nd_2Fe_{14}B$ has been marked. For searching the magnetic compounds that outperform $Nd_2Fe_{14}B$, many studies have been carried out. In terms of high $\mu_0 H_A$, compounds like $Tb_2Fe_{14}B$, Sm_5Fe_{17} exhibit values greater than 20 T. However, the $\mu_0 M_s$ of these compounds are < 0.7 T [55–57], making them unsuitable for permanent magnet applications. $Sm_2Fe_{17}N_3$ have the highest $\mu_0 H_A \sim 22$ T [21,58] but the $\mu_0 M_s$ is only 1.57 T, which is lower than the $Nd_2Fe_{14}B$. Several studies on 1:12-based compounds ($SmFe_{12}$, $NdFe_{12}N$, $Sm(Fe, Co)_{12}$, $(Sm, Zr)(Fe,Co)_{12}$) are shown to have the intrinsic magnetic properties superior to $Nd_2Fe_{14}B$. In particular, the 1:12 compounds doped with Co and Zr improved the $\mu_0 M_s$ and T_c. However, these compounds are unstable in bulk form and require stabilizing elements such as Ti and V which significantly degrades the magnetic properties, especially $\mu_0 M_s$ [6]. Thus, in the search for superior permanent magnetic compounds, a potential candidate in terms of intrinsic magnetic properties while considering the phase stability has not been demonstrated, until this work. In this study, the magnetic properties of $SmFe_9N_\delta$ ($SmFe_{8.8}N_{1.1}$) were investigated, and superior comprehensive intrinsic magnetic properties were demonstrated.

The excellent intrinsic magnetic properties of the Sm-Fe-N (1:7) phase, which are on par with the other existing Sm-Fe and RE-Fe-B-based compounds (Fig. 8), demonstrate the potential of these materials for further development. It is worth mentioning that $Sm_2Fe_{17}N_3$ and $SmFe_9N$ powders have already been commercialized by some magnet manufacturers like Daido Steel for bonded magnet fabrication [60–63]. Meanwhile, this study on demonstrating the superior intrinsic properties can accelerate the research towards further development of these compounds. However, the application to full-density bulk permanent magnets would be challenging, because the RE-Fe based nitrides tend to decompose into RE-N and α-Fe at elevated temperatures above 800 K. It is noteworthy that the Sm-Fe-N (1:7) compound has been reported to have the decomposition temperature of 920 K [7], which is slightly higher than the $Sm_2Fe_{17}N_3$ (873 K) [64] and $NdFe_{12}N_x$ (843 K) [45]. Despite this, there have been few prior successes in sintering of these nitride compounds. Sato *et al.* synthesized anisotropic Sm-Fe-N powder of 1:7 phase using a low-temperature reduction diffusion process and developed sintered magnets using the high-pressure current sintering technique with a relative density of ~ 87 % [7]. In another work, Saito *et al.* has achieved high density (>90%) in Sm-Fe-N (1:7) bulk magnets using spark plasma sintering and dynamic compression technique at temperature below 823 K [65]. It was shown that the extrinsic magnetic properties of sintered magnets do not deteriorate from the initial powder properties by successfully avoiding the decomposition of nitride powders. Recently, Takagi *et al.* followed shock-wave consolidation method for acquiring fully dense state of the Sm-Fe-N isotropic magnets and demonstrated a high-density isotropic magnet with highest level of maximum energy product (144 kJ/m^3) [62]. These studies give us an understanding that bulk magnet development is still possible in the Sm-Fe-N (1:7) compounds by sophisticated consolidation methods. Future work on sintering studies and low-temperature densification processes are necessary for developing the Sm-Fe-N (1:7) based bulk permanent magnets. Furthermore, the Sm-Fe-N (1:7) is a rare-earth lean compound where the Fe content can be increased well beyond the stoichiometric ratio (Fe:Sm ~ 10). This high Fe content can enhance the saturation magnetization beyond the existing $Nd_2Fe_{14}B$ and $Sm_2Fe_{17}N_3$, making it a potential permanent magnet candidate. Overall, this study suggests that the $TbCu_7$-type $SmFe_{\sim 9}N_\delta$ compound is a promising next generation permanent magnetic compound.

4. Conclusion

In this work, $TbCu_7$-type $SmFe_9N_\delta$ (δ=0, 0.5, 0.7 and 1.1) epitaxial thin films were synthesized and its comprehensive intrinsic magnetic properties were studied. Highly textured nature and phase purity of the $TbCu_7$-type phase in the thin film was revealed by XRD and TEM. Excellent intrinsic magnetic properties of $\mu_0 M_s = 1.64$ T, $\mu_0 H_A = 22.6$ T and $T_c = 771$ K were found for $SmFe_{8.8}N_{1.1}$. These enhanced intrinsic properties are attributed to the nitridation of 1:7 phase, wherein increasing the nitrogen content in the thin film switches the magnetocrystalline anisotropy from planar to uniaxial type with a high $\mu_0 H_A$ as

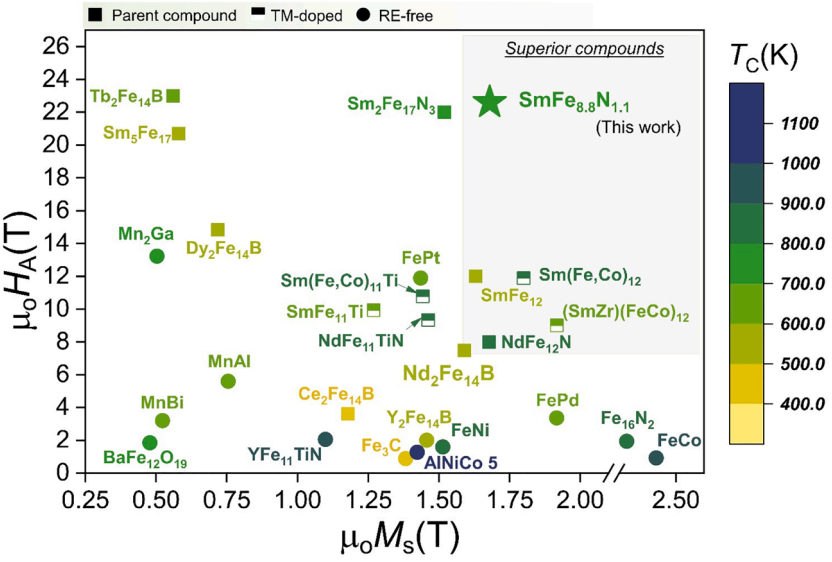

Fig. 8. Benchmark figure of intrinsic magnetic properties representing the several permanent magnetic materials realized so far along with the present work [2,11,12,21,22,43,37,46–59].

well as increases the $\mu_o M_s$ and T_c. The intrinsic magnetic properties determined for the $SmFe_{8.8}N_{1.1}$ are superior to those of the existing $Nd_2Fe_{14}B$, $Sm_2Fe_{17}N_3$ and $SmFe_{12}$ compounds. These results demonstrate the promise of the $TbCu_7$ type $SmFe_9N_\delta$ based compounds as an alternative permanent magnet material.

CRediT authorship contribution statement

A.R. Dilipan: Data curation, Formal analysis, Methodology, Writing – original draft, Visualization. **D. Ogawa:** Investigation, Methodology, Writing – review & editing. **H. Sepehri-Amin:** Funding acquisition, Investigation, Supervision, Writing – review & editing. **P. Tozman:** Writing – review & editing. **T. Hiroto:** Data curation, Methodology. **K. Hono:** Supervision. **Y.K. Takahashi:** Funding acquisition, Supervision, Writing – review & editing.

Declaration of competing interest

The authors declare the following financial interests/personal relationships which may be considered as potential competing interests

Y.K. Takahashi and H. Sepehri-Amin report financial support was provided by MEXT program: Data Creation and Utilization-Type Material Research and Development Project (JPMXP1122715503).

Acknowledgements

This work was supported in part by the MEXT program: Data Creation and Utilization-Type Material Research and Development Project (JPMXP1122715503). We acknowledge Dr. Rajkumar Modak, Dr. Varun Kushwaha and Dr. Yuya Sakuraba for the technical support on sputtering machine. A. R. Dilipan acknowledge Ms. Yukie Mori and Dr. Satoshi Sugimoto for FIB sample preparation and support on substrate preparation respectively.

Supplementary materials

Supplementary material associated with this article can be found, in the online version, at doi:10.1016/j.actamat.2024.119996.

References

[1] O. Gutfleisch, M.A. Willard, E. Brück, C.H. Chen, S.G. Sankar, J.P. Liu, Magnetic materials and devices for the 21st century: stronger, lighter, and more energy efficient, Advanced Materials 23 (2011) 821–842, https://doi.org/10.1002/adma.201002180.

[2] M. Sagawa, S. Fujimura, H. Yamamoto, Y. Matsuura, S. Hirosawa, Magnetic properties of rare-earth-iron-boron permanent magnet materials, J. Appl. Phys. 57 (1985) 4094–4096, https://doi.org/10.1063/1.334629.

[3] J.M.D. Coey, Perspective and Prospects for Rare Earth Permanent Magnets, Engineering 6 (2020) 119–131, https://doi.org/10.1016/j.eng.2018.11.034.

[4] I.M.S.K. Ilankoon, N.P. Dushyantha, N. Mancheri, P.M. Edirisinghe, S.J. Neethling, N.P. Ratnayake, L.P.S. Rohitha, D.M.D.O.K. Dissanayake, H.M.R. Premasiri, A.M.K. B. Abeysinghe, P.G.R. Dharmaratne, N.M. Batapola, Constraints to rare earth elements supply diversification: evidence from an industry survey, J. Clean. Prod. 331 (2022) 129932, https://doi.org/10.1016/j.jclepro.2021.129932.

[5] Y.K. Takahashi, H. Sepehri-Amin, T. Ohkubo, Recent advances in SmFe12-based permanent magnets, Sci. Technol. Adv. Mater. 22 (2021) 449–460, https://doi.org/10.1080/14686996.2021.1913038.

[6] K. Otsuka, M. Kamata, T. Nomura, H. Iida, H. Nakamura, Coercivities of Sm-Fe-M sintered magnets with ThMn12-type structure (M = Ti, V), Mater Trans 62 (2021) 887–891, https://doi.org/10.2320/matertrans.MT-MBW2020003.

[7] S. Sato, K. Nishikawa, E. Node, S. Okada, Development of TbCu7-type Sm-Fe-N anisotropic magnet powder and its sintered magnets, J. Alloys. Compd. 929 (2022), https://doi.org/10.1016/j.jallcom.2022.167280.

[8] Q.F. Xiao, Z.D. Zhang, T. Zhao, W. Liu, Y.C. Sui, X.G. Zhao, D.Y. Geng, Crystallographic transformations of rapidly quenched Sm10Fe90-xTix and magnetic properties of their nitrides, J. Appl. Phys. 82 (1997) 6170–6176, https://doi.org/10.1063/1.366501.

[9] Y. Sakai, R. Omatsuzawa, I. Sakazaki, S. Suzuki, H. Hashino, T. Saito, T. Iriyama, Structure comparison between Th2Zn17-type and TbCu7-type Sm-Fe intermetallic compounds and their nitrides by means of 57Fe-Mössbauer spectroscopy, Hyperfine Interact. 166 (2005) 483–487, https://doi.org/10.1007/s10751-006-9312-7.

[10] A. Teresiak, M. Kubis, N. Mattern, M. Wolf, K.-H. Muller, M. Muller, Formation of modified TbCu7 and Th2Zn17 type structures during annealing of mechanical-alloyed Sm–Fe powders, J. Alloy. Comp. 274 (1998) 284, https://doi.org/10.1016/S0925-8388(98)00571-4.

[11] P. Tozman, H. Sepehri-Amin, K. Hono, Prospects for the development of SmFe12-based permanent magnets with a ThMn12-type phase, Scr. Mater. 194 (2021), https://doi.org/10.1016/j.scriptamat.2020.113686.

[12] Y. Otani, D.P.F. Hurley, H. Sun, J.M.D. Coey, Magnetic properties of a new family of ternary rare-earth iron nitrides R2Fe17N3-δ (invited), J. Appl. Phys. 69 (1991) 5584–5589, https://doi.org/10.1063/1.347957.

[13] K.Y. Wang, Y.Z. Wang, B.P. Hu, W.Y. Lai, Magnetic properties of Sm-Fe-Ti and its nitrides with TbCu7-type structure, Physica B 203 (1994) 54–58, https://doi.org/10.1016/0921-4526(94)90276-3.

[14] T. Saito, Magnetic properties of (Sm,Zr)Fe10 and (Sm,Zr)Fe9.5Ti0.5 melt-spun ribbons, J. Magn. Magn. Mater. 542 (2022), https://doi.org/10.1016/j.jmmm.2021.168573.

[15] M. Katter, J. Wecker, L. Schultz, Structural and hard magnetic properties of rapidly solidified Sm-Fe-N, J. Appl. Phys. 70 (1991) 3188–3196, https://doi.org/10.1063/1.349302.

[16] S. Sakurada, A. Tsutai, T. Hirai, Y. Yanagida, M. Sahashi, S. Abe, T. Kaneko, Structural and magnetic properties of rapidly quenched (R,Zr)(Fe,Co)10Nx (R=Nd, Sm), J. Appl. Phys. 79 (1996) 4611–4613, https://doi.org/10.1063/1.361679.

[17] H. Saito, M. Takahashi, T. Wakiyama, Magnetic properties and structure change from tetragonal to hexagonal for the rapidly quenched SmTiFe11 alloy ribbons, J. Appl. Phys. 64 (1988) 5965–5967, https://doi.org/10.1063/1.342164.

[18] H.T. Kim, Q.F. Xiao, Z.D. Zhang, D.Y. Geng, Y.B. Kim, T.K. Kim, H.M. Kwon, Phases of melt-spun Sm1− xFe7+ x alloys and magnetic properties of their nitrides. J. Magn. Magn. Mater. 173(3), 295–301. 10.1016/S0304-8853(97)00169-8.

[19] L. Peng, Q.H. Yang, H.W. Zhang, Y.Q. Song, J. Shen, Crystal structure and magnetic properties of hard magnetic Sm2Fe17Nδ thin films with Co substitution, J. Magn. Magn. Mater. 321 (2009) 442–445, https://doi.org/10.1016/j.jmmm.2008.09.029.

[20] T. Kusumori, A. Fujita, K. Mibu, Effect of atomic modulation on the J-mixing-dominant magnetic anisotropy in SmFe7 epitaxial films, Appl. Phys. Express. 9 (2016), https://doi.org/10.7567/APEX.9.043001.

[21] T. Iriyama, K. Kobayashi, H. Kato, Y. Nakagawa, Magnetic properties of Sm2Fe17Nx, IEEE Trans. Magn. 7 (12) (1992) 924–930, https://doi.org/10.1016/0304-8853(92)90099-A.

[22] T. Iriyama, K. Kobayashi, N. Imaoka, T. Fukuda, H. Kato, Y. Nakagawa, Effect of nitrogen content on magnetic properties of Sm2Fe17Nx (0<x<6), IEEE Trans. Magn. 28 (1992) 2326–2331, https://doi.org/10.1109/20.179482.

[23] D.S. Edgley, B. Saje, A.E. Platts, I.R. Harris, The diffusion of nitrogen into Nb-modified Sm2Fe17 powder, J. Magn. Magn. Mater. 138 (1994) 6–14, https://doi.org/10.1016/0304-8853(94)90394-8.

[24] H. Fujii, K. Tatami, K. Koyama, Nitrogenation process in SmzFe17 under various N2-gas pressures up to 6 MPa, J. Alloys Compd. 236 (1996) 156–164, https://doi.org/10.1016/0925-8388(95)02080-2.

[25] O. Kurnosikov, L. Pham Van, J. Cousty, High-temperature transformation of vicinal (0001) Al2O3-α surfaces: an AFM study, Surf. Interface Anal. 29 (2000) 608–613, https://doi.org/10.1002/1096-9918(200009)29:9<608::AID-SIA906>3.0.CO;2-B.

[26] M.D. Kuz'min, Shape of temperature dependence of spontaneous magnetization of ferromagnets: quantitative analysis, Phys. Rev. Lett. 94 (2005), https://doi.org/10.1103/PhysRevLett.94.107204.

[27] T. Ono, N. Kikuchi, S. Okamoto, O. Kitakami, T. Shimatsu, Novel torque magnetometry for uniaxial anisotropy constants of thin films and its application to FePt granular thin films, Appl. Phys. Express. 11 (2018), https://doi.org/10.7567/APEX.11.033002.

[28] K.H. Müller, L. Cao, N.M. Dempsey, P.A.P. Wendhausen, Sm2Fe17 interstitial magnets (invited), J. Appl. Phys. 79 (1996) 5045–5050, https://doi.org/10.1063/1.361568.

[29] S. Isogami, Y.K. Takahashi, Antiperovskite Magnetic Materials with 2p Light Elements for Future Practical Applications, Adv. Electron. Mater. 9 (2023), https://doi.org/10.1002/aelm.202200515.

[30] K.H.J. Buschow, The importance of ternary intermetallic compounds in science and technology, J. Alloys Compd. 193 (1993) 223–230, https://doi.org/10.1016/0925-8388(93)90355-Q.

[31] J.M.D. Coey, K. O'Donnell, New bonded magnet materials (invited), J. Appl. Phys. 81 (1997) 4810–4815, https://doi.org/10.1063/1.365470.

[32] D. Ogawa, T. Yoshioka, X.D. Xu, Y.K. Takahashi, H. Tsuchiura, T. Ohkubo, S. Hirosawa, K. Hono, Magnetic anisotropy constants of ThMn12-type Sm(Fe1–xCox)12 compounds and their temperature dependence, J. Magn. Magn. Mater. 497 (2020), https://doi.org/10.1016/j.jmmm.2019.165965.

[33] P. Tozman, H. Sepehri-Amin, T. Abe, K. Hono, Y.K. Takahashi, Exploring secondary phases in the Sm–Fe–V system beneficial for coercivity, Acta Mater. 258 (2023), https://doi.org/10.1016/j.actamat.2023.119197.

[34] P. Tozman, T. Fukazawa, D. Ogawa, H. Sepehri-Amin, A. Bolyachkin, T. Miyake, S. Hirosawa, K. Hono, Y.K. Takahashi, Peculiar behavior of V on the Curie temperature and anisotropy field of SmFe12-xVx compounds, Acta Mater. 232 (2022), https://doi.org/10.1016/j.actamat.2022.117928.

[35] C. Lu, X. Hong, Z. Ding, J. Shi, X. Bao, X. Gao, J. Zhu, Phase formation and magnetic hardening mechanism of TbCu7 type Sm-Fe-N powders, J. Magn. Magn. Mater. 456 (2018) 6–10, https://doi.org/10.1016/j.jmmm.2018.01.071.

[36] A.E. Platts, I.R. Harris, J.M.D. Coey, Improvement in the cast structure of Sm2Fe17 alloys by niobium additions, J. Alloy. Comp. 185 (1992) 251–258, https://doi.org/10.1016/0925-8388(92)90473-M.

[37] Y. Hirayama, Y.K. Takahashi, S. Hirosawa, K. Hono, Intrinsic hard magnetic properties of Sm(Fe1 − xCox)12 compound with the ThMn12 structure, Scr. Mater. 138 (2017) 62–65, https://doi.org/10.1016/j.scriptamat.2017.05.029.
[38] J. Hu, K. Wang, Y. Wang, B. Hu, Z. Wang, Volume expansion and Curie temperature enhancement in rare earth-iron based nitrides with TbCu structure, J. Alloys. Compd. 292 (1999) 233–235, https://doi.org/10.1016/S0925-8388(99)00564-2.
[39] L. Wei, W. Qun, X.K. Sun, Z. Xin-Guo, Z. Zhi-Dong, X. Qun-Feng, Z. Tong, Y. C. Chuang, Structural and magnetic properties of mechanically alloyed Smx(Fe1-yCoy)100-x nitrides, Solid. State Commun. 91 (1994) 971–974.
[40] S. Suzuki, S. Suzuki, H. Yamamoto, Magnetic Properties of Melt-Spun Sm10(Fe, V)90Ny with TbCu7-Type Structure, IEEE Trans. Magn. 31 (1995) 902–905, https://doi.org/10.1109/20.364580.
[41] W. Yan, Y. Luo, G. Wu, N. Quan, H. Peng, D. Yu, Y. Yang, Controlled magnetic properties by tuning TbCu7 /Th2Zn17 phase in isotropic Sm-Fe-Nb-N compounds, J. Alloys. Compd. 741 (2018) 661–665, https://doi.org/10.1016/j.jallcom.2018.01.196.
[42] N. Kurokawa, M. Matsuura, S. Sakurada, S. Sugimoto, Enhancement of magnetic properties and microstructural changes in TbCu7-type Sm-Fe-Co-Nb-B melt-spun ribbons, J. Magn. Magn. Mater. 556 (2022), https://doi.org/10.1016/j.jmmm.2022.169414.
[43] P. Tozman, Y.K. Takahashi, H. Sepehri-Amin, D. Ogawa, S. Hirosawa, K. Hono, The effect of Zr substitution on saturation magnetization in (Sm1-xZrx)(Fe0.8Co0.2)12 compound with the ThMn12 structure, Acta Mater. 178 (2019) 114–121, https://doi.org/10.1016/j.actamat.2019.08.003.
[44] G. Saito, Y. Tamazawa, F. Nakagawa, M. Kambayashi, M. Doi, T. Shima, Magnetic properties of ThMn12-Type Sm-Rich Sm-Fe-Co thin films with v buffer layer, in: Proceedings of the 2019 IEEE 9th International Conference on Nanomaterials: Applications and Properties, NAP, Institute of Electrical and Electronics Engineers Inc., 2019, p. 2019, https://doi.org/10.1109/NAP47236.2019.216996.
[45] Y. Hirayama, Y.K. Takahashi, S. Hirosawa, K. Hono, NdFe12Nx hard-magnetic compound with high magnetization and anisotropy field, Scr. Mater. 95 (2015) 70–72, https://doi.org/10.1016/j.scriptamat.2014.10.016.
[46] Z. Shao, S. Ren, Rare-earth-free magnetically hard ferrous materials, Nanoscale Adv. 2 (2020) 4341–4349, https://doi.org/10.1039/d0na00519c.
[47] Tu Chen, W. Stutius, The phase transformation and physical properties of the MnBi and Mn 1.08 Bi compounds, IEEE Trans. Magn. 10 (3) (1974) 581–586, https://doi.org/10.1109/TMAG.1974.1058367.
[48] R.C. Pullar, Hexagonal ferrites: a review of the synthesis, properties and applications of hexaferrite ceramics, Prog. Mater. Sci. 57 (2012) 1191–1334, https://doi.org/10.1016/j.pmatsci.2012.04.001.
[49] J. Mohapatra, J.P. Liu, Rare-Earth-Free Permanent Magnets: the Past and Future, in: handbook of Magnetic Materials, Elsevier B.V. (2018) 1–57, https://doi.org/10.1016/bs.hmm.2018.08.001.
[50] J.T. Holguín-Momaca, C.J. Muñoz-Carnero, H. Sharma, C.R. Santillán-Rodríguez, J.A. Matutes-Aquino, C.V. Tomy, S.F. Olive-Méndez, Tuning the ferromagnetism of epitaxial-strained D019-Mn3Ga thin films, J. Magn. Magn. Mater. 471 (2019) 329–333, https://doi.org/10.1016/j.jmmm.2018.09.100.
[51] J. Cui, M. Kramer, L. Zhou, F. Liu, A. Gabay, G. Hadjipanayis, B. Balasubramanian, D. Sellmyer, Current progress and future challenges in rare-earth-free permanent magnets, Acta Mater. 158 (2018) 118–137, https://doi.org/10.1016/j.actamat.2018.07.049.
[52] S. Hirosawa, Permanent Magnets beyond Nd-Dy-Fe-B, IEEE Trans Magn 55 (2019), https://doi.org/10.1109/TMAG.2018.2863737.
[53] S. Hirosawa, Current status of research and development toward permanent magnets free from critical elements, J. Magnet. Soc. Jpn 39 (3) (2015) 85–95, https://doi.org/10.3379/msjmag.1504R004.
[54] Y. Otani, D.P.F. Hurley, H. Sun, J.M.D. Coey, Magnetic properties of a new family of ternary rare-earth iron nitrides R2Fe17N3−δ (invited), J. Appl. Phys. 69 (1991) 5584–5589, https://doi.org/10.1063/1.347957.
[55] S.K. Lee, B.N. Das, V.G. Harris, Magnetic structure of single crystal Tb Fe B, Appl. Phys. Lett. 99 (2011) 162510, https://doi.org/10.1016/S0304-8853(99)00519-3.
[56] S. Hirosawa, Y. Matsuura, H. Yamamoto, S. Fujimura, M. Sagawa, H. Yamauchi, Magnetization and magnetic anisotropy of R2Fe14B measured on single crystals, J. Appl. Phys. 59 (1986) 873–879, https://doi.org/10.1063/1.336611.
[57] I. Dirba, H. Sepehri-Amin, K. Skokov, Y. Skourski, K. Hono, O. Gutfleisch, Magnetic properties and microstructure of Sm5Fe17-based composite magnets, Acta Mater. 212 (2021), https://doi.org/10.1016/j.actamat.2021.116912.
[58] J.M.D. Coey, P. Stamenov, S.B. Porter, M. Venkatesan, R. Zhang, T. Iriyama, Sm-Fe-N revisited; remanence enhancement in melt-spun Nitroquench material, J. Magn. Magn. Mater. 480 (2019) 186–192, https://doi.org/10.1016/j.jmmm.2019.02.076.
[59] T. Iriyama, The discovery of Sm2Fe17N3 permanent magnet material, J. Jpn Soc. Powder Powder Metall. 43 (1996) 59–65, https://doi.org/10.2497/jjspm.43.59.
[60] Sakazaki, Iwao. "Sm—Fe—N magnet material and Sm—Fe—N bonded magnet." U. S. Patent No. 11,742,121. 29 Aug. 2023.
[61] Sakazaki, Iwao, and Takefumi Sugiyama. "Sm-Fe-N magnet material and Sm-Fe-N bonded magnet." U.S. Patent No. 10,658,095. 19 May 2020.
[62] S. Takagi, K. Morii, T. Iriyama, K. Tominaga, N. Wada, E. Hida, Y. Yamada, Evaluation of practicality for fully dense isotropic sm-fe-n magnets made by shock-wave consolidation method, IEEE Trans. Magn. (2023) 59, https://doi.org/10.1109/TMAG.2023.3283997.
[63] J.M.D. Coey, T. Iriyama, J. Croat, J. Ormerod, Chapter 09 - Bonded Sm-Fe-N permanent magnets. Modern Permanent Magnets, Woodhead Publishing, 2022, pp. 305–342, https://doi.org/10.1016/B978-0-323-88658-1.00008-X.
[64] N. Imaoka, K. Takagi, K. Ozaki, T. Iriyama, H. Kato, Thermal stability of Sm2Fe17N3 magnet powders. J. Phys. Conf. Ser., Institute of Physics Publishing, 2017, https://doi.org/10.1088/1742-6596/903/1/012042.
[65] T. Saito, K. Kikuchi, Production of Sm–Fe–N bulk magnets by the spark plasma sintering method with dynamic compression, J. Alloys. Compd. 673 (2016) 195–198, https://doi.org/10.1016/j.jallcom.2016.02.240.